IAEA nuclear fusion

ACCEPTED MANUSCRIPT • OPEN ACCESS

Plasma self-driven current in tokamaks with magnetic islands

To cite this article before publication: Weixing Wang *et al* 2024 *Nucl. Fusion* in press https://doi.org/10.1088/1741-4326/ad8f45

Plasma self-driven current in tokamaks with magnetic islands

W. X. Wang[1], M. G. Yoo[2], E. A. Startsev[1], S. Kaye[1], S. Ethier[1], J. Chen[1]

[1] Plasma Physics Laboratory, Princeton University, P.O. Box 451, Princeton, NJ 08543, USA

[2] General Atomics, San Diego, CA 92121

E-mail: wwang@pppl.gov

July 2024

Abstract. Magnetic island perturbations may cause a reduction in plasma self-driven current that is needed for tokamak operation. A novel effect on tokamak self-driven current revealed by global gyrokinetic simulations is due to magnetic-island-induced 3D electric potential structures, which have the same dominant mode numbers as that of the magnetic island, whereas centered at both the inner and outer edge of the island. The non-resonant potential islands are shown to drive a current through an efficient nonlinear parallel acceleration of electrons. In large aspect ratio (large-A) tokamak devices, this new effect can result in a significant global reduction of the electron bootstrap current when the island size is sufficiently large, in addition to the local current loss across the island region due to the pressure profile flattening. It is shown that there exists a critical magnetic island width for large-A tokamaks beyond which the electron bootstrap current loss is global and increases rapidly with the island size. As such, this process may introduce a size limit for tolerable magnetic islands in large-A tokamak devices in the context of steady state operation. On the other hand, the current loss caused by magnetic islands in low-A tokamaks such as spherical tokamak (ST) NSTX/U is minor. The reduction of the axisymmetric current by magnetic islands scales with the square of island width. However, the loss of the current is mainly local to the island region, and the pace of current loss as the island size increases is substantially slower compared to large-A tokamaks. In particular, the bootstrap current reduction in STs is even smaller in the reactor-relevant high-β_p regime where neoclassical tearing modes are more likely to develop.

PACS numbers: 52.55.-s, 52.65.-y, 52.25Fi, 52.55Fa, 52.65.Tt

1. Introduction

Tokamak devices rely on electric current carried by the plasma itself in the toroidal direction for producing a poloidal magnetic field necessary for plasma confinement, unlike stellarator devices where electric currents provided by external coils are used to produce helical magnetic field for confinement. The plasma current in tokamaks can be driven in several ways. First, and most common, is electromagnetic induction as in transformers. In this case, the plasma acts as the secondary winding of the transformer. The use of inductive current in tokamaks leads to pulsed operation because of finite magnetic flux swing and finite conductivity. Steady state tokamak operation preferred for fusion reactors requires stationary current which can be driven non-inductively by radio-frequency waves and neutral beams. These external drivers of non-inductive current are also widely used in tokamak experiments. In addition to externally driven current, plasmas can also produce self-driven current, such as the well-known bootstrap current [1, 2, 3] driven along the magnetic field by pressure and temperature gradients in the perpendicular direction. This current originates from the diamagnetic effect associated with particle drift orbits in the toroidal magnetic field, along with friction between trapped and passing particles due to Coulomb collisions. In the presence of a pressure gradient, the neoclassical diamagnetic effect of magnetically trapped particles produces an asymmetry in the trapped particle velocity distribution function $f(v_\parallel)$, and collisional deflection of trapped particles into passing particles produces net parallel drift motion of passing particles [4], leading to the bootstrap current. Another self-driven current contribution comes from anomalous current driven by plasma turbulence due to various micro-instabilities. The turbulence driven current generation has drawn strong interests in theory, simulation and experiment [5, 6, 7, 8]. More recently, a new type of plasma current was observed in KSTAR experiment under conditions with particle fueling and minimal externally driven and bootstrap currents [9], though the origin of the current remains to be identified.

The prediction of bootstrap current is a major result of neoclassical theory developed in plasma physics [1, 2, 10]. It was observed and confirmed experimentally more than a decade later [3, 11, 12]. Plasma self-generated non-inductive current plays a fundamental role in tokamak-based fusion experiments, as recognized early on when the bootstrap current was discovered [2]. Because external drivers of non-inductive current are very expensive, commercial grade tokamak reactors will largely rely on plasma self-driven current for generating the poloidal magnetic field needed for steady state operation [13, 14]. The self-driven current also strongly affects key magnetohydrodynamic (MHD) instabilities, such as the neoclassical tearing modes (NTM) [15, 16, 17] and edge localized modes (ELM) [18, 19, 20].

Magnetic islands that are often generated by internal MHD instabilities or external perturbations in fusion plasmas are likely unavoidable in long pulse discharges. Changes in magnetic topology by magnetic islands can have strong and complex effects on both neoclassical and turbulent dynamics (including bootstrap current generation) in tokamaks [21], which are axisymmetric by design. Magnetic islands are often observed to cause confinement degradation. Large uncontrolled islands even lead to plasma disruption [22]. On the other hand, some improved confinement state due to internal transport barrier formation inside a rational magnetic surface is linked to the presence of a magnetic island at the surface [23, 24, 21]. Magnetic islands usually lead to a bootstrap current reduction. However, it is generally understood that the current loss is mainly due to pressure profile flattening across the island and limited to the island region. In fact, experimental observations suggest that magnetic islands have additional effects on plasma current. In the hybrid scenario experiments, the presence of magnetic islands is shown to non-locally modify current and q profile in the core through the so-called current profile broadening effect [25]. This phenomenon plays a critical role in mitigating the sawtooth instability for hybrid discharges [25, 26, 27, 28].

This paper reports on an extensive simulation study of tokamak self-generated current in the presence of magnetic islands, emphasizing the consistent calculation associated with the effects of the magnetic-island-induced three-dimensional ambipolar equilibrium electric field. A novel effect due to nonlinear parallel acceleration of electrons by the magnetic-islands-induced non-resonant electric potential islands is found to drive a significant parallel current, modifying the tokamak self-driven current. Depending on magnetic island size and tokamak aspect ratio, the new effect may cause a global reduction in the bootstrap current. Given that a significant self-driven current reduction could jeopardize the economic viability of a tokamak-based fusion reactor, the simulation results suggest that there may exist a size limit for tolerable magnetic islands in large-aspect-ratio tokamaks in the context of steady state operation beyond which the electron bootstrap current loss is global and increases rapidly with the size of the islands. On the other hand, the current loss caused by magnetic islands in low-A tokamaks [e.g., spherical tokamak (ST) such as NSTX/U] is minor, suggesting a favorable feature of STs for non-inductive steady state operation and for developing compact fusion reactors.

The rest of the paper is organized as follows: In Sec. 2, formulated problems and simulation model for this study are described. The simulation study for large aspect ratio tokamaks is introduced in Sec. 3. This includes the results of the magnetic island induced 3D potential structures, a new electron current driven by the 3D potential via nonlinear parallel acceleration and the dependence of the current reduction on island size. In Sec. 4, modifications of plasma self-driven current by magnetic islands in STs (NSTX/U) are discussed. In Sec. 5, the electron current loss by the presence of magnetic island is calculated and compared for different tokamak experiments, highlighting a favorable feature for STs. In Sec. 6, conclusions are given, and implications and connections of the findings from this study to experimental observations are discussed.

2. Problem formulation and simulation model

Here our goal is to compute the neoclassical equilibrium solution in island geometry with a consistent electric field in order to investigate comprehensive effects associated with magnetic island perturbations on neoclassical processes and bootstrap current. The equilibrium electric field in toroidal plasmas is determined by the neoclassical process through the ambipolarity of particle transport [29]. It is well-known that the neoclassical radial electric field can have a major influence on micro-instabilities (and associated turbulence-driven transport) through its $\mathbf{E} \times \mathbf{B}$ shear flow [30]. The equilibrium electric field may also affect ion neoclassical transport through the squeezing of ion orbit width

[31, 29]. In general, however, the effects of equilibrium E_r on neoclassical transport in axisymmetric tokamaks are not so significant and often neglected. This includes its effect on the bootstrap current [32]. However, the equilibrium electric field may have more important and direct effects on neoclassical dynamics in 3D geometry. It is noticed that 3D electrostatic potential variations may need to be kept when calculating neoclassical effects in stellarators [33].

This computational study employs a global gyrokinetic model to solve for the neoclassical equilibrium using an initial value approach [29, 32]. The model consists of gyrokinetic ions and drift kinetic electrons, and the governing kinetic equations and gyrokinetic Poisson equation (charge neutrality condition), which determines electric potential self-consistently, are solved using the δf particle-in-cell method [34]. This allows us to calculate a 3D neoclassical equilibrium electric field in 3D perturbed tokamak geometry with magnetic islands. The use of gyrokinetic ions, that are required in turbulence simulations when the perpendicular scale length of fluctuation potential is comparable to the ion gyroradius, is retained here, though it is not not strictly essential for this problem. The change of $\mathbf{E}\times\mathbf{B}$ structure due to magnetic islands is shown to have a strong impact on turbulence and the associated transport in island geometry [21]. The 3D ambipolar potential in the stochastic magnetic field that arises to maintain the quasi-neutrality of the plasma is found to provide a key collisionless mechanism for energy transport along the stochastic magnetic field lines responsible for the thermal quench in major tokamak disruptions [35, 36]. The inclusion of a consistent 3D electric field is also critical for calculating the tokamak self-driven current in the presence of magnetic islands.

In order to obtain a quantitative understanding of island impacts on tokamak self-driven current, simulations presented in this paper are carried out with real experimental discharges. The simulations cover various plasmas of both large aspect ratio and low-aspect ratio spherical tokamaks, including a C-MOD Ohmic plasma, an NSTX-U L-mode and an NSTX high-β_p H-mode plasma. Experimental plasma parameters used in the simulations include electron and ion density and temperature profiles and reconstructed MHD equilibrium based on pressure and current profiles. A prescribed magnetic island is imposed as MHD perturbations to the reconstructed axisymmetric tokamak equilibrium.

Specifically, a magnetic island perturbation used in the simulations is described by an analytic model [37]

$$\delta\mathbf{B} = \nabla\times\alpha B_0, \quad \alpha = \alpha_{mn} sin(n\phi - m\theta),$$

for 3D perturbed magnetic field, where B_0 is the unperturbed axisymmetric equilibrium magnetic field, and m, n are the poloidal and toroidal mode numbers of the island. The magnetic perturbation of the island is dominated by the radial component. This expression describes an m/n-island located at the rational surface where the safety factor $q(r) = m/n$. The island width estimated in terms of the radial coordinate of poloidal flux ψ_p is $\Delta\psi_p = 4\sqrt{\alpha_{mn}/s}$, which depends on the magnetic shear s and is proportional to the square root of the perturbation amplitude δB.

3. Magnetic-island-induced potential and effect on electron current in large-aspect ratio tokamaks

For large-A tokamak cases, a C-MOD Ohmic L-mode discharge is used as a base plasma (with aspect ratio=3.3, elongation=1.6 and triangularity=0.49). This discharge has ITG-dominated turbulence in the core plasma. However, turbulence effects are not the focus of this study, and thus, are excluded in the simulations. This C-MOD discharge has a monotonic q-profile as shown in Fig.1, and a m/n=2/1 magnetic island is imposed on the $q = 2$ surface located at the normalized minor radius $r/a = 0.61$. The Poincare plot in Fig.1 shows a 2/1 magnetic island used in the simulations with the C-MOD discharge. To focus on the effects of the magnetic islands, toroidal rotation is set to zero in the simulations. The global simulations cover a radial domain from $r/a = 0.2$ to 0.9. The plasma temperature and density profiles are set to be flat in both inner and outer radial boundary regions ($r/a < 0.35$ and $r/a > 0.75$) compatible with the boundary conditions used in the simulations.

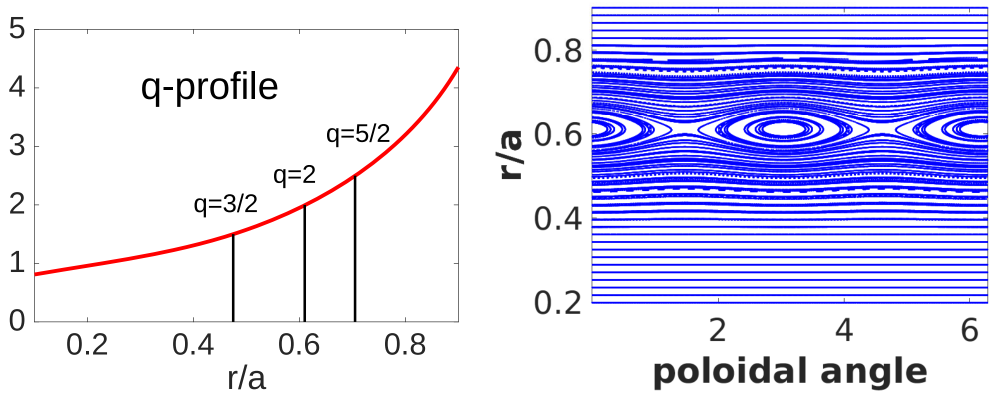

Figure 1. q-profile of a C-MOD L-mode plasma (left); Poincare plot (right) showing an imposed 2/1 island centered at $q = 2$ (at the normalized minor radius $r/a = 0.61$) in the simulations.

The typical amplitude of magnetic island perturbations present in confined plasma is small, e.g., $\delta B/B_0 \sim 10^{-4}$. However, magnetic islands introduce changes in the topological structure of the confining magnetic field, which may introduce strong and complex effects on plasma transport and confinement in toroidal devices. In the case of tokamaks, 3D perturbations of magnetic islands cause toroidal asymmetry which may significantly change the neoclassical equilibrium including equilibrium electric field. As part of this process, this paper examines its effect on the bootstrap current. Our focus is on the bootstrap current carried by electrons, which is most strongly affected by the presence of magnetic islands, and on the axisymmetric component of the current, which is what contributes to the generation of poloidal magnetic field for tokamak operation.

3.1. Island-induced 3D electric field and nonlinear parallel acceleration driven current

First, a well-known effect of magnetic islands is to modify plasma profiles through fast parallel streaming of particles along the perturbed magnetic field lines, leading to fast equilibration of plasma across the island region. Correspondingly, the plasma pressure profile flattens across the island region. The process of the temperature and density flattening during the evolution of the island system towards the new equilibrium is illustrated in Fig.2, top panels, which show the spatio-temporal evolution of electron temperature (left panel) and density (right panel) variations. In this simulation, only the radial component of the electric field (rather than the fully 3-dimensional electric field) is included. This is done by solving the flux-surface-averaged charge neutrality condition. Note that the electron temperature and density equilibration processes occur at different time scale. The temperature flattens at a much faster time scale which is associated with electron parallel dynamics characterized by electron thermal speed. The electron density, on the other hand, flattens at a slower time scale associated with ion dynamics characterized by ion sound speed. This is because the electron density equilibration process must be constrained by the transport ambipolarity or charge neutrality condition, and the associated ambipolar electric field couples the density equilibration process to ion dynamics, which is much slower.

The radial profile of electron density and temperature at the new equilibrium state (after many electron collision times) are plotted in the lower-left panel of Fig.2. Both electron temperature and density are significantly modified across the island region, while they remain almost unchanged in the other regions due to a low rate of neoclassical transport for electrons. Corresponding to the island-modified neoclassical equilibrium, the lower-right panel of Fig.2, which plots and compares the radial profiles of flux-surface-averaged electron current density $\langle j_{e,\parallel} B\rangle$ from the simulations with and without the magnetic island, shows how the electron bootstrap current is modified. Concurrently, the electron bootstrap current in the island center is significantly reduced due to the electron profile flattening effect across the island center. There are two localized spikes appearing in the electron current profile at both the inner and outer edges of the island, which correspond to the electron profile steepening at two locations as seen on the lower-left of Fig.2. Basically, the modification of the electron current is local to the island region, following the island-induced electron profile modifications. In this case, the electron current is reduced but remains finite.

However, this conventional picture of loss of bootstrap current in the presence of magnetic island is incomplete. A magnetic island, by changing magnetic topological structure, may have a profound influence on the neoclassical equilibrium electric field. In axisymmetric equilibrium, neoclassical particle transport is intrinsically ambipolar in the first order of ion orbit width (part of the standard neoclassical theory). The ambipolar neoclassical electric field is determined by transport effects of higher order in particle orbit width [29], and is largely dominated by the radial component. The breaking of tokamak axisymmetry by magnetic perturbations, such as magnetic islands,

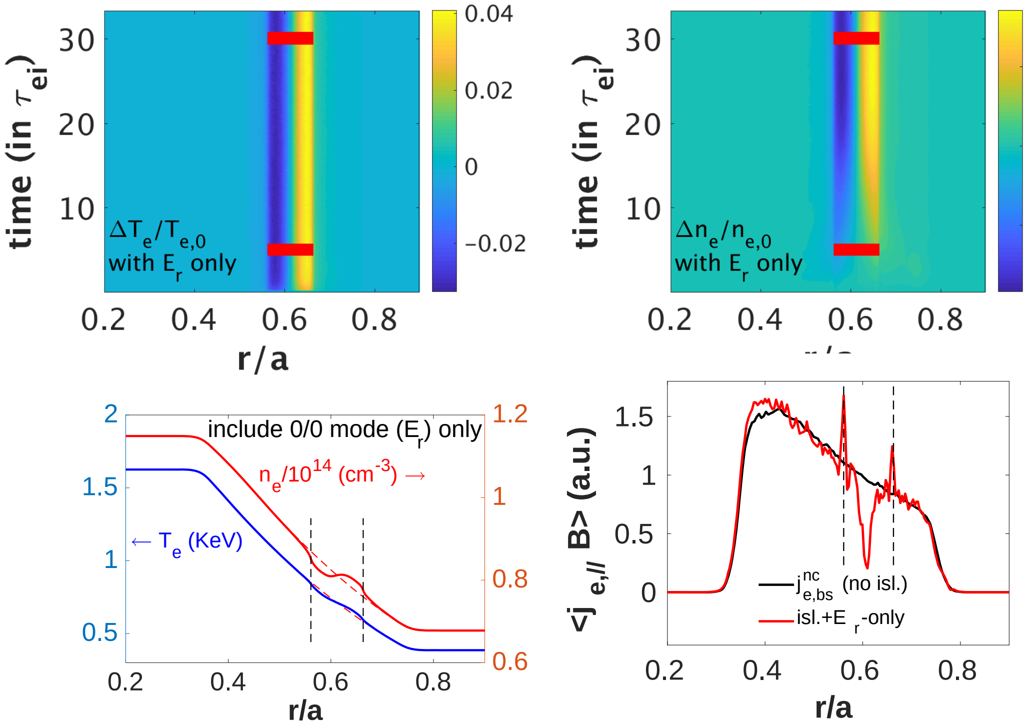

Figure 2. Radial-temporal evolution of simulated electron temperature change $\Delta T_e/T_{e,0}$ (upper-left) and electron density change $\Delta n_e/n_{e,0}$ (upper-right), with red bars indicating the location and width of the magnetic island; Steady state electron temperature and density profile (solid lines) in comparison with the original profiles with no island (dashed lines) (lower-left); simulated electron current density profile with island (red) and without island (black) (lower-right). Black vertical dashed lines indicate boundaries of the island.

also breaks the intrinsic ambipolarity of the low order neoclassical transport. As such, magnetic island perturbations not only change the equilibrium radial electric field, but also introduce new features in the neoclassical electric field.

The island perturbations turn the radially dominant equilibrium electric field into a 3-dimensional one. The 3-dimensional equilibrium electric field obtained from our simulation is presented in Fig.3. In the simulation, we only retain low-n components of the electric potential from n=0 to 4, and filter out all the high-n modes that may be driven by micro-instabilities, such as ion temperature gradient modes (ITG) and trapped electron modes (TEM). Notice that in this plasma the low-n modes ($n = 0-4$) are stable to ITG and TEM instabilities. Instead, they are determined by the neoclassical effect as the 3D ambipolar electric field in the simulation. First, the presence of magnetic island perturbations is shown to cause a significant change in the equilibrium radial electric field in tokamak geometry, as shown in the left of Fig.3. Compared to the axisymmetric tokamak case with no magnetic perturbation, the magnetic island is found to cause a major change in the plasma equilibrium from a weak negative E_r to a positive one, resulting in an E_r-well across the magnetic island with radial extension into the inner side of the island.

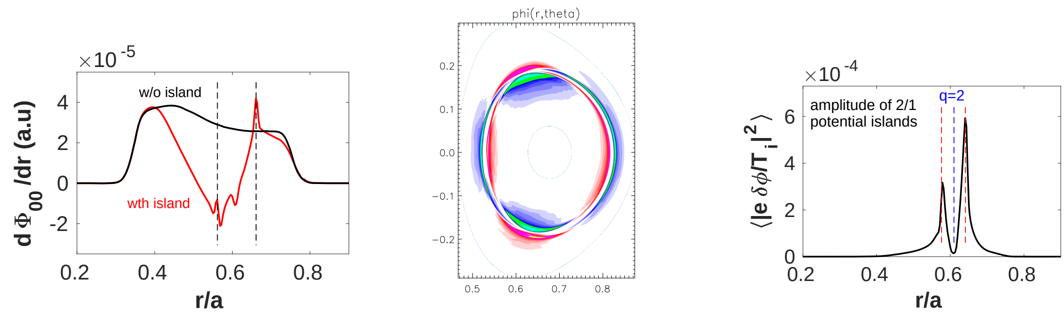

Figure 3. Profile of equilibrium radial electric field calculated at steady state (left); contour plot of non-zonal potential, showing magnetic-island-induced potential islands with red and blue colors representing positive and negative potentials, respectively (middle); radial profile of potential island amplitude, showing they are centered on the inner and outer boundary of the magnetic island (right). Vertical red dashed lines indicate location and width of magnetic island.

A fundamental change associated with the presence of magnetic islands in tokamaks is that the ambipolar electric field becomes 3-dimensional. In addition to the change in the E_r profile, a magnetic island is shown to drive electric potential islands. The contour plot of the simulated low-n electric potential excluding m/n=0/0 component (i.e., E_r component), clearly shows island structures (middle of Fig.3). The low-n potential islands are dominated by m/n=2/1 modes, the same mode numbers as that of the magnetic island. Unlike the magnetic island, the 2/1 potential islands, however, are centered at both the inner and outer edge of the magnetic island. This is clearly shown by the radial profile of potential islands' amplitude $\langle|e\delta\phi/T_i|^2\rangle$ plotted in the right of Fig. 3. In axisymmetric tokamaks (with no MHD perturbations), a poloidal component in equilibrium electric field may be generated by the centrifugal-force-induced charge separation when the plasma is rotating toroidally [38]. However, the associated poloidal electric field is much smaller than the radial electric field. In contrast, the amplitude of potential islands induced by magnetic islands can be higher than that of typical turbulence and increases as the island width increases. The potential islands contribute to a significant 3D electric field at a level comparable to that of the radial electric field.

The island-induced 3D ambipolar electric field, which is dominated by 2/1 potential islands in the C-MOD plasma case of our simulations, is found to produce a major change in the plasma self-driven current. Here we compare the results of the two neoclassical simulations: the first one includes solely the radial electric field, while the second includes the full 3-dimensional electric field. As shown in Fig. 4 (left panel), the two simulations produce almost identical electron temperature and density profiles at the island equilibrium state, which account for the magnetic island-induced modification.

However, the simulation with full 3D electric field produces a highly different electron parallel current (right panel of Fig.4). The large change in the electron current appears not only in the island region, but also globally. Apparently, this major change is not related to the island-induced electron pressure profile change. Across the island region (as indicated by the two dashed lines) where the electron density and temperature profiles are modified by the island, the loss of electron bootstrap current is increased, though the electron profile modifications looks almost identical to that of the simulation with E_r only. In the inner and outer sides of the island where the electron profiles are unmodified by the island, a significant electron current reduction and increase are observed, respectively, when we calculate the consistent full 3D electric field in the simulation. In particular, a large electron current loss occurs in the inner core region next to the magnetic island. Two localized electron current spikes in both inner and outer edges of the island in the current profile are visible in both cases, reflecting the electron profile steepening at the two locations.

The results of these two simulations clearly show a strong influence of island-induced electric field on the parallel current. The change in the electron current $j_{\|,e}$ is linked to electron parallel momentum transport and flow generation [6, 39, 40, 41, 42] in the presence of 3D electric field perturbations, and can be described by the following equations,

$$\frac{\partial\langle\Delta j_{\|,e}\rangle}{\partial t} + \nabla\cdot\langle\delta v_{E\times B} j_{\|,e}\rangle = -\frac{e^2}{m_e}\langle\delta E_\|\delta n_e\rangle + \nu_{ei}\langle\Delta j_{\|,e}\rangle. \quad (1)$$

Here, the last term on the right is the resistive current damping due to collisions. A 3D electric field perturbation may modify the electron current via two effects. The second term on the left of Eq.1 is due to the well-known cross-field flux of the electron parallel momentum associated with the $\vec{E}\times\vec{B}$ drift $\delta v_{E\times B}$. The radial flux of the parallel momentum can lead to the radial redistribution of electron parallel current density while not changing the total electron current. The first term on the right of Eq.1 is produced by the nonlinear beating between perturbations of parallel electric field $\delta E_\|$ and density δn_e, representing a nonlinear parallel acceleration of electrons [43, 44, 39]. This effect originates from a wave-induced momentum exchange between electrons and ions [45]. While it does not change the total momentum of ions and electrons, the momentum transfer from ions to electrons may effectively induce an electron current because of the large ion-to-electron mass ratio. For the magnetic island induced non-resonant potential island perturbations, the $\vec{E}\times\vec{B}$ generated flux of parallel momentum is negligible. The change in electron parallel current is found to be mainly driven by the nonlinear parallel acceleration of electrons by the non-resonant potential islands. Figure 5 shows the spatio-temporal evolution of the current change $\partial\langle j_{\|,e}\rangle/\partial t$ and the parallel acceleration $\langle\delta E_\|\delta n_e\rangle$. These two quantities in Eq. 1 show an apparent correlation in spatio-temporal structures during the development of the electron current, suggesting that the nonlinear parallel acceleration drives electron current generation. It is seen from quasi-linear analysis that the nonlinear parallel acceleration by the potential perturbations is sensitive to the asymmetry in the potential amplitude around a rational surface [40, 41], namely between $|\phi_{k_\parallel}|^2$ and $|\phi_{-k_\parallel}|^2$, where $k_\parallel = \frac{m-nq}{qR_0}$ is the parallel wave-number. A similar effect associated with turbulent potential fluctuations appears in turbulence driven current generation [7]. For typical turbulence in fusion plasmas produced by drift wave instabilities such as ion temperature gradient mode (ITG) and trapped electron mode (TEM), modes with $+k_\parallel$ and $-k_\parallel$ are equally excited around the mode rational surface in ideal situations, namely, the mode is symmetric around the rational surface $|\phi_{k_\parallel}|^2 = |\phi_{-k_\parallel}|^2$. Therefore, physical effects that can cause the breaking of the $k_\parallel$-symmetry of the turbulence modes play a critical role for the nonlinear parallel acceleration to drive a current. There are various symmetry breaking mechanisms, such as $\mathbf{E}\times\mathbf{B}$ flow shear [46, 47], turbulence intensity gradient [48], turbulence self-generated low frequency zonal flow shear [49], and up-down asymmetry in magnetic geometry [50] etc. Unlike turbulence-driven potential perturbations, the potential islands induced by magnetic island are non-resonant and intrinsically asymmetric. This feature, in principle, makes it efficient for potential islands to drive an electron current.

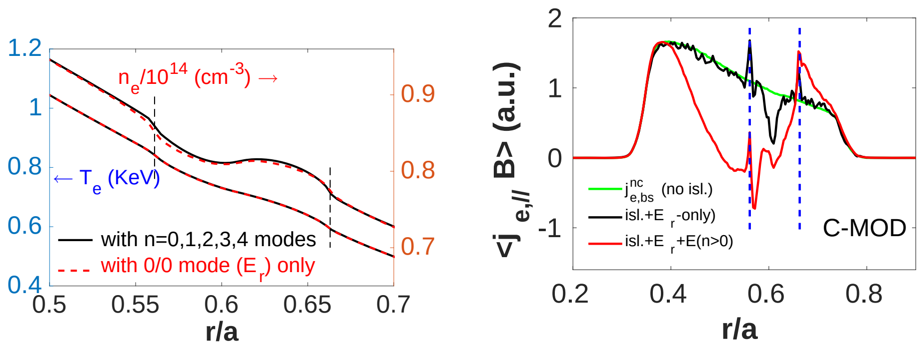

Figure 4. Radial profiles of electron temperature and density (left) and electron parallel current (right) from two simulations with one including solely E_r and another including full 3D electric field.

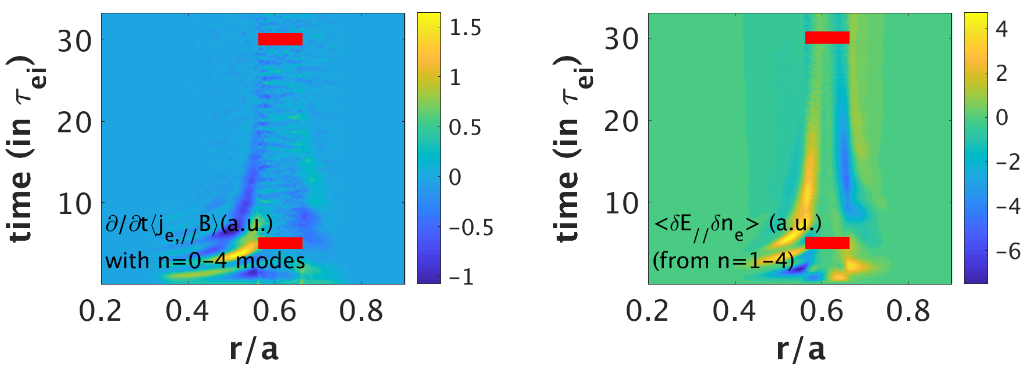

Figure 5. Spatio-temporal evolution of $\partial\langle j_{\parallel,e}B\rangle/\partial t$ (left) and electron parallel acceleration $\langle\delta E_\parallel \delta n_e\rangle$ (right).

The electron current reaches a steady state during the simulations as the neoclassical equilibrium state of electrons is established in the island geometry. As shown in left panel of Fig. 6, which is the evolution of a simulated electron current density profile, the electron current reaches the neoclassical equilibrium state in a few tens of electron collision times. The right panel of Fig. 6 plots the radial profile of the equilibrium electron current density induced by the effects associated with magnetic island for a C-MOD case (red curve), which is calculated as the difference between the simulated electron currents with and without a magnetic island i.e., $\Delta\langle j_{\|,e}B\rangle = \langle j_{\|,e}B\rangle - \langle j_{bs,e}B\rangle$. In the steady state, an electron current driven by the nonlinear parallel acceleration due to the potential islands is determined by the balance between the current driven by the nonlinear parallel acceleration and the resistive decay due to collisional damping [43], and can be estimated accordingly from

$$\nu_{ei}\langle\Delta j_{\|,e}\rangle \approx -\frac{e^2}{m_e}\langle\delta E_{\|}\delta n_e\rangle,$$

where ν_{ei} is the electron collision frequency, e and m_e are electron charge and mass, respectively. Note that electron perturbations are divided into adiabatic and non-adiabatic responses, and both adiabatic and non-adiabatic electrons contributions to this part of the electron current are estimated separately in terms of their corresponding distribution functions,

$$\langle\delta E_{\|}\delta n_e^{ad}\rangle = \langle\delta E_{\|}(e\delta\phi/T_e)n_0\rangle \ \text{ and } \ \langle\delta E_{\|}\delta n_e^{non-ad}\rangle = \langle\int \delta E_{\|}\delta h_e dv^3\rangle,$$

and are plotted by the blue and black curve in Fig.6 (right panel), respectively. As seen in the figure, the current driven by the potential islands through the nonlinear parallel acceleration is shown to account for both the electron current loss in the inner core region and gain in the outer core region next to the magnetic island, where the electron density and temperature profiles are almost unmodified by the magnetic island. Moreover, the parallel acceleration current is almost fully contributed by non-adiabatic electron response. In the region across the magnetic island, the modification of the electron current comes from the contributions of multiple physics effects including the pressure profile flattening and the parallel accelerations.

3.2. Dependence of current reduction on island size

Now we examine the dependence of the island-induced electron current loss on the size of magnetic island. To this end, a set of simulations with different island sizes are performed. It is found that the modification to the electron current profile by this new effect shows remarkably sensitive dependence on the size of the island in large-aspect ratio tokamaks. The left panel of Fig. 7 shows the simulated electron current profiles from three simulations with 2/1 islands of different island size (with their corresponding island widths indicated by the vertical dash lines) for the same C-MOD discharge. For the smaller island, the island-induced current loss mainly appears in the island region (black curve), and the effect associated with the 3D potential is small. As island size increases, the current loss not only gets deeper in the island region, but also extends

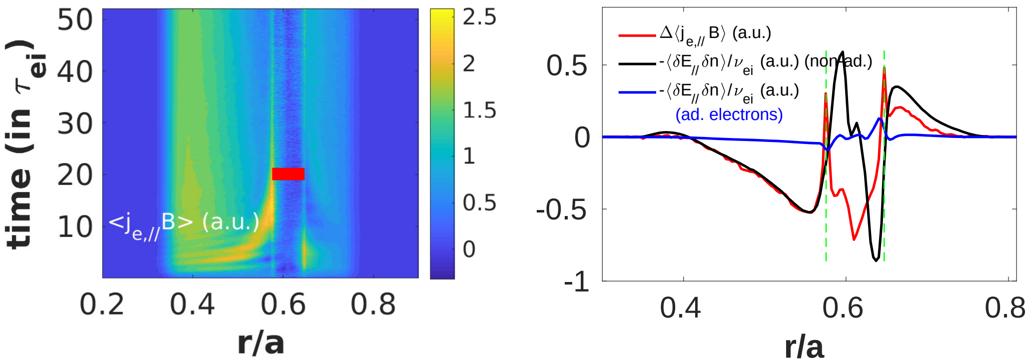

Figure 6. Spatio-temporal evolution of of electron current density $\langle j_{\|,e}B\rangle$ (left); radial profiles of equilibrium electron current change due to magnetic island $\Delta\langle j_{\|,e}B\rangle = \langle j_{\|,e}B\rangle - \langle j_{bs,e}B\rangle$; and the current associated with the nonlinear parallel acceleration (right).

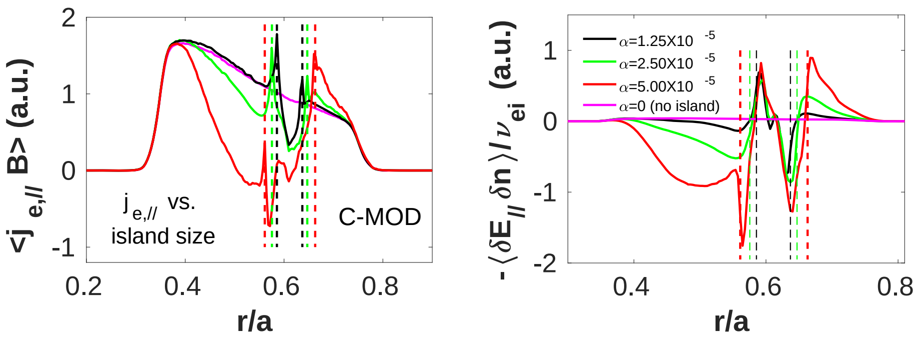

Figure 7. Radial profiles of simulated equilibrium electron current for large-A tokamak (C-MOD case) with three different island sizes, showing a change in the current loss from local to global as island size increases (left); radial profiles of parallel acceleration current of three corresponding island sizes (right). Also plotted is the results of simulation with no magnetic island perturbations.

into the inner core region. In the meantime, a positive electron current is driven by the 3D potential in the outer region next to the island, adding to the electron bootstrap current in the region. Plotted in the right panel of Fig. 7 is the evaluation of nonlinear parallel acceleration driven currents of three corresponding island sizes, where the size dependence shown in the parallel acceleration driven current consistently accounts for the results of simulated electron current in the left of Fig.7. As a cross check of the simulation, also plotted in Fig. 7 are the results of a simulation with no magnetic island perturbations (pink curves). In the simulation, the non-axisymmetric component of ambipolar potential is also calculated, which is shown in a negligible noise level (as it is supposed to be in axisymmetric tokamaks) and does not drive a noticeable electron current.

Simulations to scan the dependence of the island-induced current change on the

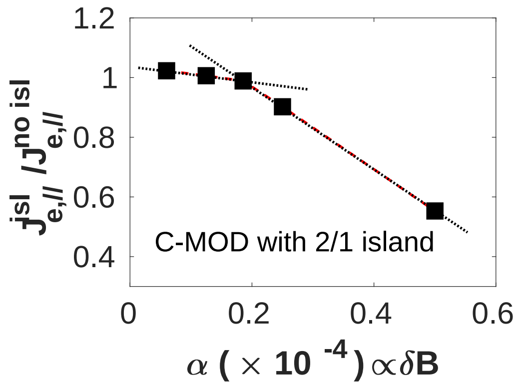

Figure 8. Total electron current normalized by the electron bootstrap current with no magnetic island vs. magnetic island perturbation amplitude.

amplitude of magnetic island perturbations were performed and the results are presented in Fig.8 which is the total electron current (volume-integrated) normalized by the total electron bootstrap current without magnetic island vs. $\alpha \propto \delta B$. It is shown that the total electron current decreases linearly with the increase of magnetic island perturbation amplitude δB. Interestingly, the linear decrease of electron current with δB appears to have a different slope, depending on the range of δB amplitude. For smaller island sizes the slope is weak. In the range of larger island sizes the slope is steeper, and the increased current loss with island size is due to a global extension of current loss into the inner core region driven by the parallel acceleration effect. The results suggest that there exists a critical value of magnetic island size for the electron current loss. Specifically for the C-MOD case presented here, the critical island size roughly corresponds to the cross point of the two straight lines in Fig.8. Below the critical size, the current loss is local and minor. Beyond the critical size, the current loss is global and significant, and rapidly increases with the magnetic island size.

It is highly instructive to compare the phase space structure of the electron distribution function with and without magnetic island. This type of study may provide physical information at a fundamental level with regard to how the electron current is modified by magnetic islands. Presented in Fig. 9 are electron distributions $\delta f_e(v_\parallel, v_\perp)$ for three different island sizes. To be precise, the distribution functions are calculated at minor radius $r/a = 0.5$ and mid-plane $\theta = 0$ and averaged in toroidal direction. At this radial location, the electron current is substantially reduced when the island size is sufficiently large (see the right of Fig. 7). First, the asymmetry in $\delta f_e(v_\parallel, v_\perp)$ with respect to $v_\parallel = 0$ in the case of no magnetic island (left of Fig. 9) is a direct illustration of a net electron current (i.e., the neoclassical bootstrap current). Both the positive δf_e in $v_\parallel < 0$ domain and the negative δf_e in $v_\parallel > 0$ domain contribute a positive current (along B-direction). The distribution function does not change considerably when the island size is small (middle of Fig. 9), and consequently, the electron current loss at this radial location is small. When the island becomes sufficiently large, the electron distribution is significantly distorted at the location (right of Fig. 9), even though T_e and n_e remain unchanged. In particular, the large positive δf_e in the $v_\parallel < 0$ domain that contributes a positive bootstrap current in the case with no island is largely diminished, leading to a reduction in the current at the location.

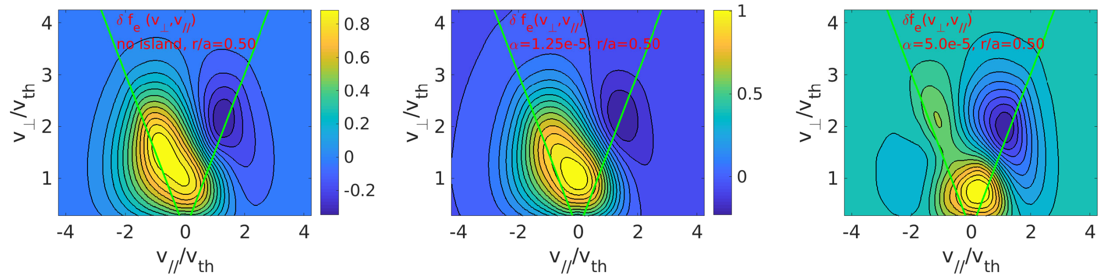

Figure 9. Electron distribution function $\delta f_e(v_\parallel, v_\perp)$ (large-A C-MOD case) with no magnetic island (left), small island (middle) and large island (right) in the core region ($r/a = 0.5$ – inside the island radial location) where a substantial electron current loss occurs when the island size is sufficiently large. The two straight lines in each plot indicate the boundary between trapped and passing electrons.

The significant reduction of the parallel current when a magnetic island is sufficient large could be observed in experiments, though direct measurements of tokamak self-driven current are difficult [usually, total plasma current (sum of all current contributions and volume-integrated) is measured in experiments]. A favorable situation for detecting this new effect in tokamaks is discharges with a high fraction of bootstrap current. A significant modification of bootstrap current with respect to the neoclassical value can be reflected in a change of q-profile which can be directly measured. Stellarators which are designed to have little bootstrap current could also be ideal experiments to detect the magnetic-island-induced plasma current that is reported here. In fact, a change in current profile in the presence of a magnetic island has long been observed in hybrid scenario tokamak experiments (see Sec. 6 for more discussions). In addition, a large depletion of parallel current may drive a magnetic island size change and impact the Ohmic return current – those can be interesting issues for further investigation.

4. Modification of plasma self-driven current by magnetic islands in spherical tokamaks (NSTX/U)

Low-aspect ratio spherical tokamak experiments explore significant variations in plasma parameter space towards fusion energy production with a compact design to reduce cost compared to that of conventional large-aspect ratio tokamaks. STs, such as the National Spherical Torus eXperiment (NSTX) [51] and its upgrade NSTX-U, are characterized by high-β (the ratio of plasma pressure to magnetic pressure), large ρ^* (the ratio of ion gyroradius to the plasma minor radius), strong toroidicity and shaping, etc. Such highly distinct features result in a different tokamak plasma regime with some unique physics properties, including transport and confinement behaviors, compared to conventional tokamaks[51, 52]. A prominent key feature that was observed in NSTX H-mode plasmas is a favorable energy confinement scaling with the collisionality, e.g., $B_T\tau_E \propto 1/\nu_{*,e}$ [52], where τ_E, $\nu_{*,e}$ and B_T are the energy confinement time, electron collisionality and toroidal magnetic field, respectively. This scaling predicts a higher performance for ST devices relative to conventional tokamaks in high temperature burning plasma regime. This scaling will be further tested in the lower $\nu_{*,e}$ regime of the NSTX-U experiment.

Like in large-A tokamaks, maintaining operation at large bootstrap fraction required for non-inductive and low-disruptivity steady state operation is critical for compact fusion devices. Now we extend our investigation to ST plasmas. The simulation study is applied first to an NSTX-U L-mode discharge (with aspect ratio=1.8, elongation=1.7 and triangularity=0.35). This discharge has a monotonic q-profile and we impose a 2/1 magnetic island at $q = 2$ surface (see left panel of Fig.11 for the q-profile). Similar to the large-A tokamak case, the 2/1 magnetic island is shown to drive non-resonant electric potential islands as part of the 3D ambipolar electric field (see lower-right of Fig. 10). As usual, the electron pressure profile is relaxed to become flat across the island region in the island equilibrium state due to the fast free streaming of electrons along the perturbed magnetic field lines, as illustrated in the lower-left of Fig. 10, and the pressure profile flattening is mostly contributed by electron density profile relaxation. Again, the equilibrium electron profiles in the regions outside the island is unaffected. The modification of electron current in the presence of magnetic island, however, appears to be significantly different than that of large-A tokamak cases, as shown in the upper-left of Fig. 10 which is the calculated electron current profiles of two simulations with different island sizes. The loss of the electron current is shown mainly in the island region. Unlike in the case of large-A tokamaks, a strong current loss in the inner core region (where the electron temperature and density profiles are unmodified) is not observed in ST plasmas even with a large magnetic island. Interestingly, we see an enhancement of electron current instead in the inner core region next to the island. The effect of the electron parallel acceleration caused by the 3D equilibrium electric field is estimated (upper-right of Fig. 10), which is shown to drive a positive electron current in the region. This appears to be the cause of the electron current increase as observed in the inner core region. As such, the overall current loss by the magnetic island is significantly weaker relative to that of large-A tokamaks.

The effect of magnetic islands on tokamak self-driven current matters mostly for high-β_p plasmas operating in the regime with a large bootstrap current fraction critical for the development of non-inductive, economic fusion reactors. On the other hand, NTM islands are more likely to develop in high-β_p plasmas. To this end, our simulation study is applied to an NSTX high-β_p H-mode discharge [53]. Because of the elevated q-profile of the high-β_p plasma (see left of Fig. 11), we impose a m/n=4/1 magnetic island at the $q = 4$ surface at normalized minor radius $r/a = 0.48$ (rather than a 2/1 island in the previous cases of C-MOD discharge). The presence of a 4/1 magnetic island

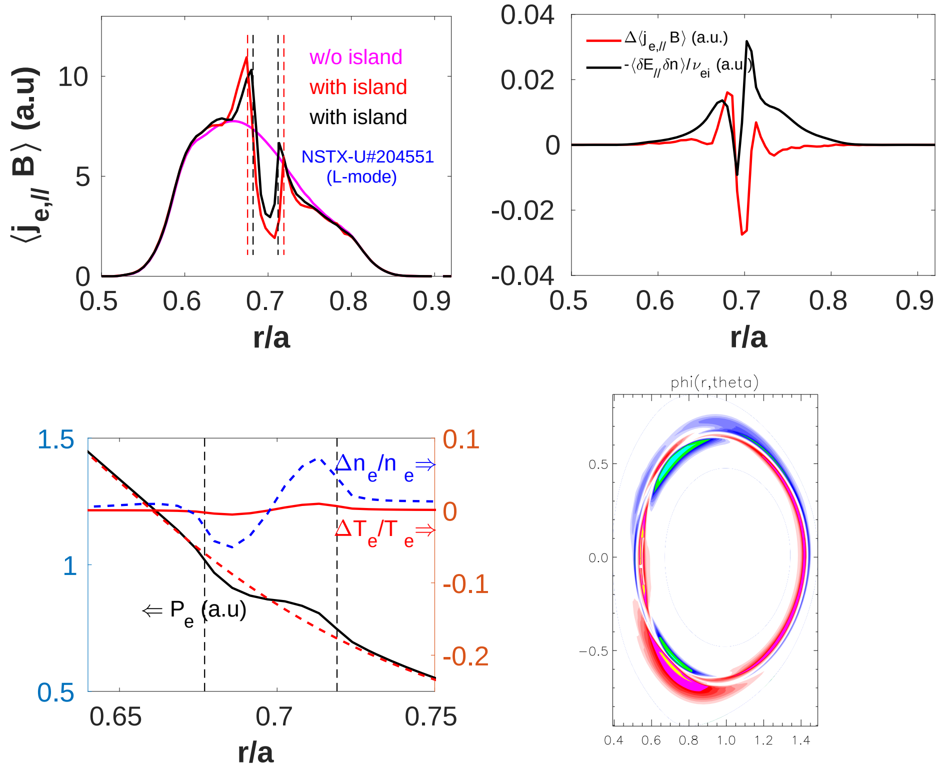

Figure 10. Radial profiles of simulated equilibrium electron current for an NSTXU L-mode case with two different island sizes (upper-left); magnetic island induced electron current $\Delta\langle j_{\|,e}B\rangle = \langle j_{\|,e}B\rangle - \langle j_{bs,e}B\rangle$, and an estimate current driven by nonlinear parallel acceleration (for a smaller island case) (upper-right); electron pressure profile and n_e and T_e changes at island equilibrium state (lower-left); contour plot of potential island on a poloidal plane (for a larger island case) (lower-right).

induces non-resonant potential islands with the dominant mode numbers the same as 4/1, as shown in the right of Fig. 11. In the middle panel of Fig. 11, which is the simulated electron current profiles for two cases (varying island perturbation δB by a factor 2), the electron current loss is shown to occur only locally in the island region, while additional current is driven in both the inner and outer core regions adjacent to the magnetic island, which compensates for the current loss in the island region, leading to a total current loss being minor. Note that the island model used in our simulations appears to generate small harmonic perturbations at other radial locations in high-β_p plasmas, which may also produce small and highly localized modifications to electron current at the radii in the simulation (see middle of Fig.11).

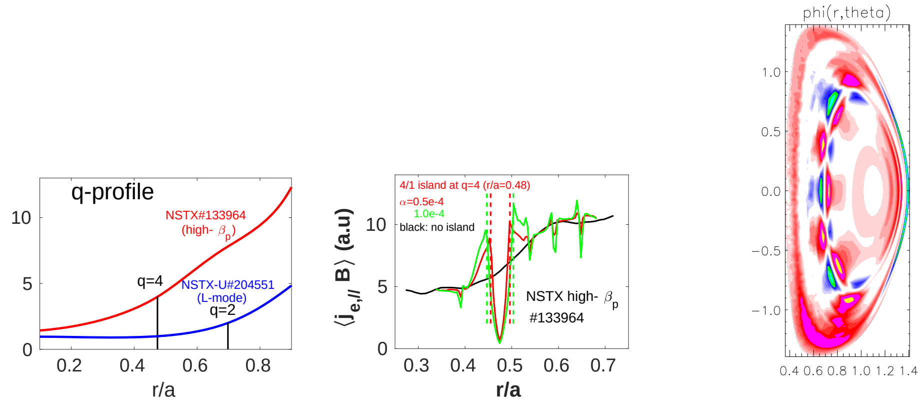

Figure 11. The q-profiles of an NSTX high-β_p and an NSTXU L-mode plasma (left); Radial profiles of simulated electron current with two different island sizes (middle) and 4/1 magnetic-island-induced potential islands for the NSTX high-β_p plasma.

5. Dependence of electron current loss on magnetic island size in different plasmas

Now we compare the impact of magnetic islands on the bootstrap current in different tokamak plasmas. Systematic simulation scans varying the perturbation amplitude δB ($\propto \alpha_{mn}$) of the magnetic islands have been performed for the three plasmas to characterize the dependence of the magnetic-island-induced current loss on island size. The simulation results are summarized in Fig. 12, which plots the total electron current (volume-integrated current) normalized by the corresponding electron bootstrap current with no island vs. island size measured in terms of perturbation amplitude (left panel) and normalized island width (right panel). For large aspect tokamaks, a dramatic current loss may occur when the magnetic island perturbation amplitude is larger than a critical value for which the magnetic island induced non-resonant potential islands can drive a strong negative electron current in the broad inner core region. In NSTX/U, the new effect of magnetic island on bootstrap current is much weaker. The reduction of the axisymmetric current by the magnetic island scales with the square of island width which is $\propto \sqrt{\delta B/s}$ (Fig. 12, left). However, the loss of the current is mainly local in the island region, and the pace of the current loss as the island size increases is substantially slower compared to large-aspect ratio tokamaks. In the reactor-relevant high-β_p regime where NTM islands are more likely to develop, the bootstrap current reduction by magnetic islands in STs is even smaller. These results of the comparison between large-A and low-A tokamaks are further elaborated by plotting the normalized current loss as a function of island size in terms of the normalized island width by the machine minor radius in the right of Fig. 12. It clearly shows that the pace of bootstrap current loss with the increase of normalized magnetic island width is slowest in ST high β_p regime. It should be noted that the comparison between the C-MOD 2/1 island case and the NSTX 4/1 island case may not be a fair one. However, we emphasize some qualitative differences between large-A and low-A. For the low-A, for both the 2/1 and 4/1 island cases, the loss of the electron current is limited in the island region, and an enhancement of the current in the inner core region next to the islands is observed, in contrast to a strong current loss in the same region for the large-A geometry. Further, from simple calculations of island width normalized by minor radius vs. perturbation amplitude normalized by B_0 between large-A and low-A geometry from the island model we used, it is noticed that, for the same level of magnetic perturbations $\delta B/B_0$, MHD island width is significantly smaller in the NSTX/U plasmas than in the large-A C-MOD plasma (as indicated in Fig. 12, right). Specifically, for the 2/1 island cases, a large island perturbation ($\delta B/B_0 \sim 1.4\%$) in NSTX gives a current loss at a level comparable to that of a much smaller island perturbation ($\delta B/B_0 \sim 0.2\%$) in C-MOD (see right plot of Fig. 12). The combination of these contrasted results between the large- and low-A geometries suggests a favorable feature of STs for non-inductive steady state operation and for developing compact fusion reactors.

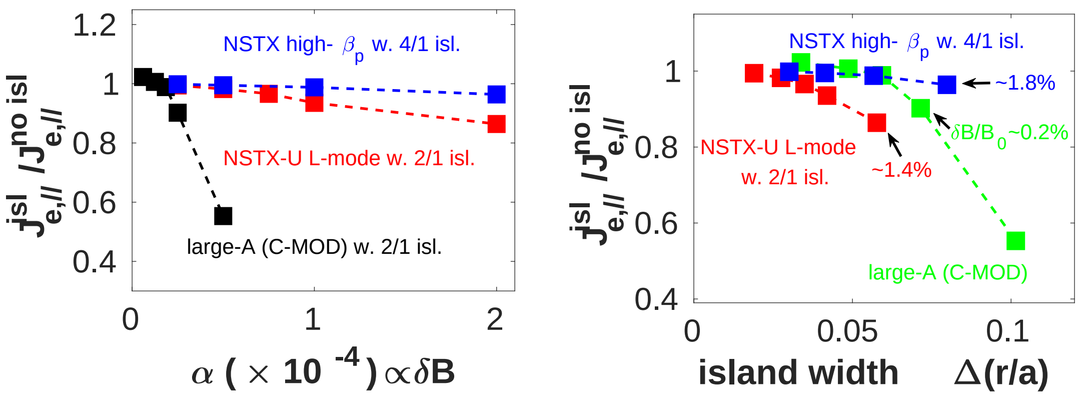

Figure 12. Total electron current normalized by its bootstrap current without island vs island perturbation amplitude δB (left) and island width normalized by the minor radius (right) for three different plasmas.

6. Discussion and conclusions

In this paper, tokamak self-driven current generation in the presence of magnetic islands has been investigated through a gyrokinetic simulation that calculates global neoclassical equilibrium and consistent 3D equilibrium electric field. Our focus is on the axisymmetric current that concerns the tokamak operation by producing a steady state poloidal magnetic field needed for plasma confinement. The simulation study has revealed a novel effect associated with magnetic island induced 3D equilibrium electric field that can significant change the tokamak self-driven current. A magnetic island is shown to drive potential islands centered at the inner and outer edges of the magnetic island, which turns the radially dominated equilibrium electric field in axisymmetric tokamak geometry into a 3D electric field. The associated parallel electric field can produce an effective acceleration for electrons via nonlinear beating with density perturbations, which drives an electron parallel current. The nonlinear parallel acceleration driven current may result in a significant reduction in the electron current, depending on tokamak aspect ratio and magnetic island size. In large aspect ratio tokamaks, there exists a critical island size for electron current loss. When the magnetic island size is greater than the critical island size, the nonlinear parallel acceleration can drive a strong negative current in a wide inner core region, leading to a global reduction to the electron bootstrap current in addition to the current loss across the island region due to the pressure profile flattening. In this regime, the electron current loss increases rapidly with the magnetic island size. This result may have an important implication to the steady state operation of tokamak devices that require non-inductive plasma current instead of Ohmic current which is pulsed. For an economic operation of tokamak-based reactors, a high fraction of tokamak self-driven current, mainly from the bootstrap current, is preferred. The existence of a critical magnetic island size beyond which the electron current loss increases dramatically may introduce a size limit for a tolerable magnetic island in large aspect ratio tokamaks in the context of steady state operation.

On the other hand, for low aspect ratio tokamaks, specifically for the spherical tokamaks NSTX/U that we have investigated here, this new effect on the electron current is found to be different and the island-induced current loss is much weaker. Regardless of the island size, the electron current loss happens mainly in the island region, while a positive electron current due to the nonlinear parallel acceleration is observed in the outer regions adjacent to the magnetic island, which makes up for some of the current loss in the island region. The overall bootstrap current reduction scales with the square of the island width in ST plasmas, but with a much slower pace compared to that of large aspect ratio tokamaks. Unlike in the large aspect ratio case, there is no critical magnetic island size observed for characteristic change in the current loss. Finally, the current loss of ST devices in more reactor-relevant high-β_p regime is shown to be minor with the slowest pace among the different plasmas examined in this study. These results suggest a favorable feature of STs for non-inductive steady state operation and for developing compact fusion reactors.

The finding that a magnetic island may induce a nonlocal current loss in the core plasma inside the island location may have a significant implication and connection to some experimental phenomena. In fact, a change in current profile in the presence of a magnetic island is widely observed in tokamak experiments. This phenomenon plays a critical role in accessing the hybrid operation scenario with no sawtooth in various tokamak devices [28]. In DIII-D, the development of hybrid plasmas is often accomplished by the emergence of m/n=3/2 NTM island [25, 27, 26] which could be excited by the edge localized modes (ELMs) or sawteeth. It is believed that the presence of a 3/2 magnetic island in these plasmas is responsible for raising the core q-profile from below 1 to ≥ 1, leading to the stabilization of the sawtooth instability. First, in DIII-D hybrid plasmas with a m/n=3/2 magnetic island, the measured central q_{min}-value is consistently higher that the simulation which assumes standard neoclassical bootstrap current. This discrepancy in q_{min} between the measurement and the simulation indicates an overestimated plasma current in the core region [27]. Further, by applying electron cyclotron current drive (ECCD) at the co- or counter-direction to shrink or expand NTM island size [54], it is observed that the q-value at the magnetic axis increases with the NTM island width [26]. In a general terminology, the underlying process responsible for these observations is loosely referred to the poloidal "magnetic-flux pumping" which causes a broadening of the current density profile [25]. However, the detailed physics picture of the process in connection to the presence of magnetic island is not well discussed or elaborated. The result reported in this paper that a magnetic island can induce a global loss of bootstrap current in the core inside the island resonant magnetic surface provides a clear picture to elucidate the process of the current profile broadening and the associated q-profile change in the hybrid plasmas with magnetic islands. The trend dependence of current loss on the island size due to this new effect shown in Fig. 8 is consistent with the trend observed in experiments (e.g., Fig. 8 of ref. [26]).

Ongoing and future work will focus on the following studies. i) It is highly interesting to investigate the impact of island-induced loss in tokamak self-driven current in low-collisionality regime relevant to high temperature burning plasmas due to this newly revealed effect. ii) The simulation study will be extended to high-β_p plasmas of large aspect ratio tokamaks as the issue matters most significantly in such situations. iii) Simulations will be applied to the hybrid plasmas to make a quantitative assessment of this new effect on the current density profile and q-profile in order to establish a more direct physics connection to the experimental observations. Finally, it is also highly interesting to assess this new effect in future reactor-scale tokamaks (such ARC, STEP and FPP concepts at various aspect ratio). This could be an additional design parameter to take into account. Given that gyrokinetic calculations for this problem are quite computational intensive, developing reduced models for an effective evaluation of island-induced plasma current will be useful for integrated modeling of existing and future devices. Such reduced models could be derived from this work based on the key physics of nonlinear parallel acceleration, taking into account geometry effects, such as plasma shaping, aspect ratio, collisionality, etc.

Acknowledgments

This work was supported by U.S. DOE Contract DE-AC02-09CH11466, Long Pulse Tokamak Scenario & Control on KSTAR Project and SciDAC Tokamak Disruption Simulation Project, and used resources of U.S. DOE NERSC computer facility under award ERCAP0024673.

References

[1] Galeev A A and Sageev R Z 1968 *Sov. Phys.JETP* **26** 233
[2] Bickerton R J, Conner J W and Taylor J B 1971 *Nature Phys. Sci.* **229** 100
[3] Zarnstorf M C and Prager S C 1984 *Phys. Rev. Lett.* **53** 454
[4] Hirshman S and Sigmar D 1981 *Nucl. Fusion* **21** 1079
[5] McDevitt C J, Tang X Z and Guo Z 2013 *Phys. Rev. Lett.* **111** 205002

[6] Wang W X, Ethier S, Hinton F L, Hahm T S, Boozer A, Diamond P H, Tang W M and Li Z Q 2012 Turbulence generated non-inductive current and flow shear driven turbulent transport in tokamaks *Proc. 24th Int. Conf. on Fusion Energy Conference (San Diego, 2012)* pp TH/P7–14 (www–naweb.iaea.org/napc/physics/FEC/FEC2012/index.htm)

[7] Wang W X, Hahm T S, Startsev E A, Ethier S, Chen J, Yoo M G and Ma C 2019 *Nucl. Fusion* **59** 084002

[8] Li E *et al.* 2022 *Phys. Rev. Lett.* **128** 085003

[9] Na Y S, Seo J, Lee Y, Choi G, Park M, Park S, Yi S, Wang W, Yoo M G, Cha M, Kim B, Lee Y H, Han H, Kim B, Lee C, Kim S, Yang S, Byun C S, Kim H S, Ko J, Lee W and Hahm T S 2022 *Nature Communications* **13** 6477

[10] Hinton F L and Hazeltine R D 1976 *Rev. Mod. Phys.* **48** 239

[11] Zarnstorf M C and Prager S C 1986 *Phys. Fluids* **29** 298

[12] Kikuchi M and Azumi M 1995 *Plasma Phys. Control. Fusion* **37** 1215

[13] Kikuchi M 1993 *Plasma Phys. Control. Fusion* **35** B39

[14] Kikuchi M and Azumi M 2012 *Rev. Mod. Phys.* **84** 1807

[15] Qu W X and Callen J D 1985 *University of Wisconsin Plasma Report No. UWPR 85-5*

[16] Carrera R, Hazeltine R D and Kotschenreuther M 1986 *Phys. Fluids* **29** 899

[17] Chang Z, Callen J D, Fredrickson E D, Budny R V, Hegna C C, McGuire K M, Zarnstorff M C and group T 1995 *Phys. Rev. Lett.* **74** 4663

[18] Zohm H 1996 *Plasma Phys. Control. Fusion* **38** 1213

[19] Xu X Q, Ma J F and Li G Q 2014 *Phys. Plasmas* **21** 120704

[20] Leonard A W 2014 *Phys. Plasmas* **21** 090501

[21] Wang W X, Yoo M G, Startsev E, Ethier S and Chen J 2021 Effects of magnetic islands on plasma confinement and self-driven current generation *Proc. 28th Int. Conf. on Fusion Energy Conference (virtual, 2021)* pp TH/4–3

[22] Hender T C *et al.* 2007 *Nucl. Fusion* **47** S128

[23] Ida K *et al.* 2004 *Phys. Plasmas* **11** 2551

[24] Kenmochi N, Minami T, Mizuuchi T, Takahashi C, Weir G M, Nishioka K, Kobayashi S, Nakamura Y, Okada H, Kado S, Yamamoto S, Ohshima S, Konoshima S, Ohtani Y and Nagasaki K 2020 *Sci. Rep.* **10** 5

[25] Petty C C, Austin M E, Holcomb C T, Jayakumar R J, Haye R J L, Luce T C, Makowski M A, Politzer P A and Wade M R 2009 *Phys. Rev. Lett.* **102** 045005

[26] Wade M R, Luce T C, Jayakumar R J, Politzer P A, Hyatt A W, Ferron J R, Greenfield C M, Murakami M, Petty C, Prater R, DeBoo J, Haye R L, Gohil P and Rhodes T 2005 *Nucl. Fusion* **45** 407

[27] Petty C C, Kinsey J E, Holcomb C T, DeBoo1 J C, Doyle E J, Ferron1 J R, Garofalo1 A M, Hyatt A W, Jackson G L, Luce T C, Murakami M, Politzer P and Reimerdes H 2016 *Nucl. Fusion* **56** 016016

[28] Luce T C *et al.* 2014 *Nucl. Fusion* **54** 013015

[29] Wang W X, Hinton F L and Wong S K 2001 *Phys. Rev. Lett.* **87** 055002

[30] Hahm T S and Burrell K H 1995 *Phys. Plasmas* **2** 1648

[31] Shaing K C and Hazeltine R D 1992 *Phys. FluidsB* **4** 2547

[32] Wang W X, Rewoldt G, Tang W M, Hinton F L, Manickam J, Zakharov L E, White R B and Kaye S 2006 *Phys. Plasmas* **13** 082501

[33] Calvo I, Parra F I, Velasco J L and Alonso J A 2017 *Plasma Phys. Control. Fusion* **59** 055014

[34] Wang W X, Ethier S, Ren Y, Kaye S, Chen J, Startsev E, Lu Z and Li Z Q 2015 *Phys. Plasmas* **22** 102509

[35] Yoo M G, Wang W X, Startsev E, Ma C H, Ethier S, Chen J and Tang X Z 2021 *Nucl. Fusion* **61** 126036

[36] Yoo M G, Wang W X, Startsev E, Ma C H, Ethier S, Chen J and Tang X Z 2022 *Phys. Plasmas* **29** 072502

[37] White R 2013 *Theory of Toroidally Confined Plasmas, 3rd ed* (Singapore: World Scientific Publishing Company)

[38] Hinton F L and Wong S K 1985 *Phys. Fluids* **28** 3082

[39] Hinton F, Waltz R E and Candy J 2004 *Phys. Plasmas* **11** 2433

[40] Garbet X, Esteve D, Sarazin Y, Dif-Pradalier G, Ghendrih P, Grandgirard V, Latu G and Smolyakov A 2014 *J. Phys.: Conf. Ser.* **561** 012007

[41] McDevitt C J, Tang X Z and Guo Z 2017 *Phys. Plasmas* **24** 082307

[42] He W, Wang L, Peng S, Guo W and Zhuang G 2018 *Nucl. Fusion* **58** 106004

[43] Itoh S I and Itoh K 1988 *Phys. Letters A* **127** 267

[44] Sugama H and Horton W 1995 *Phys. Plasmas* **2** 2989

[45] Wang L and Diamond P 2013 *Phys. Rev. Lett.* **110** 265006

[46] Dominguez R and Staebler G M 1993 *Phys. Fluids B* **5** 3876

[47] Gurcan O D, Diamond P H, Hahm T S and Singh R 2007 *Phys. Plasmas* **14** 042306

[48] Gurcan O D, Diamond P H, Hennequin P, McDevitt C J, Garbet X and Bourdelle C 2010 *Phys. Plasmas* **17** 112309

[49] Wang W X, Hahm T S, Ethier S, Rewoldt G, Lee W, Tang W M, Kaye S M and Diamond P H 2009 *Phys. Rev. Lett.* **102** 035005

[50] Camenen Y, Peeters A G, Angioni C, Casson F J, Hornsby W A, Snodin A P and Strintzi D 2009 *Phys. Plasmas* **16** 062501

[51] Ono M *et al.* 2000 *Nucl. Fusion* **40** 557

[52] Kaye S M, Gerhardt S, Guttenfelder W, Maingi R, Bell R E, Diallo A, LeBlanc B P and Podesta M 2013 *Nucl. Fusion* **53** 063005

[53] Gerhardt1 S P, Fredrickson, Gates D, Kaye S, Menard J, Bell M, Bell1 R, Blanc B L, Kugel H and Sabbagh S 2011 *Nucl. Fusion* **51** 033004

[54] Gantenbein G, Zohm H, Giruzzi G, Gnter S, Leuterer F, Maraschek M, Meskat J and Yu Q 2000 *Phys. Rev. Lett.* **85** 1243